# Growth and characterization of thin anodic oxide films on n-InSb(100) formed in aqueous solutions

Santinacci, L.; Sproule, G. I.; Moisa, S.; Landheer, D.; Wu, X.; Banu, A.; Djenizian, T.; Schmuki, P.; Graham, M. J.



**Publisher's version / Version de l'éditeur:**
https://doi.org/10.1016/j.corsci.2003.11.003
*Corrosion Science, 46, 8, pp. 2067-2079, 2004-08*

Available online at www.sciencedirect.com
SCIENCE DIRECT®
Corrosion Science 46 (2004) 2067–2079
CORROSION SCIENCE
www.elsevier.com/locate/corsci

# Growth and characterization of thin anodic oxide films on n-InSb(1 0 0) formed in aqueous solutions

L. Santinacci [a,1], G.I. Sproule [b], S. Moisa [b], D. Landheer [b], X. Wu [b], A. Banu [b,2], T. Djenizian [a], P. Schmuki [a,*], M.J. Graham [b]

[a] *Department of Materials Science (LKO), University of Erlangen–Nuremberg, Martensstrasse 7, D-91058 Erlangen, Germany*
[b] *National Research Council of Canada (NRC), Institute for Microstructural Sciences, Ottawa, Ont., Canada K1A 0R6*

Received 23 June 2003; accepted 6 November 2003
Available online 10 February 2004

**Abstract**

Anodic oxide films were galvanostatically grown on n-InSb(1 0 0) surfaces at various pH in sodium hydroxide (0.1 M NaOH, pH = 13), borate buffer (0.075 M $Na_2B_4O_7$ + 0.3 M $H_3BO_3$, pH = 8.4) and phosphate buffer (0.3 M $NH_4H_2PO_4$, pH = 4.4). Thickness, composition and morphology of the oxide films were determined by various surface analytical techniques such as Auger electron spectroscopy, X-ray photoelectron spectroscopy, scanning and transmission electron microscopy and atomic force microscopy. The oxides comprise mainly $In_2O_3$ and $Sb_2O_3$ and the oxide thickness increases with pH. Electrical properties of oxides indicate that the films may be useful as insulators in some device applications.


* Corresponding author. Tel.: +49-9131-852-7575; fax: +49-9131-852-7582.
*E-mail address:* schmuki@ww.uni-erlangen.de (P. Schmuki).
[1] On leave from: Swiss Federal Institute of Technology Lausanne (EPFL), Inst. of Materials Science, Lausanne, Switzerland.
[2] On leave from: University Politehnica, Bucharest, Romania.

0010-938X/$ - see front matter 
doi:10.1016/j.corsci.2003.11.003

## 1. Introduction

The III–V compound semiconductors are promising components of modern technology devices. Because of their direct band gap, semiconductors such as GaAs, InP and InSb are used for instance for light-emitting diodes, lasers and detectors [1–3]. Due to its narrow band gap (0.17 eV at room temperature), InSb is an important representative of this semiconductor group with wide applications in IR emission and detection [4,5] and in metal oxide semiconductor field effect transistors (MOSFETs) devices [6].

The growth of dielectric layers on semiconductors is a crucial step in semiconductor device fabrication. In contrast to Si, III–V compound semiconductors do not have the ability to form high quality thermal oxides which make their use difficult in MOS devices. Plasma oxidation of III–V compound semiconductors was also shown not to lead to suitable dielectric layers (in the case of InSb see e.g. Ref. [7]) while anodic oxidation was successfully used for several materials such as GaAs, AlGaAs or InP (see e.g. Refs. [8–10]). The anodic oxide layers have exhibited good dielectric properties opening new perspectives for the use of these materials for gate insulation and surface passivation [11–13]. InSb oxide was mainly grown in acid glycol water (AGW) [14–16] and KOH [17,18]. Chemical analysis has shown that the films are composed mainly of $In_2O_3$ and a variable amount of different antimony oxides and sometimes some Sb islands. It was observed that the dielectric properties were strongly linked to the composition of the oxide film. In the case of thermal oxidation a large amount of metallic Sb between the film and the bulk InSb causes a lower resistivity of the film.

Therefore, in the present work anodic oxide films grown on n-InSb in aqueous solutions are investigated. The influence of the electrolyte composition, pH, current density and oxidation time on the chemical composition, thickness, morphology and dielectric properties of the oxide layers was studied by Auger electron spectroscopy (AES), X-ray photoelectron spectroscopy (XPS), complemented by atomic force microscopy (AFM), transmission electron microscopy (TEM) and scanning electron microscopy (SEM), and electrical measurements.

## 2. Experimental

The material studied was n-type InSb(1 0 0) undoped ($4–6\times10^{14}$ carriers $cm^{-3}$) and doped with Te ($3–5\times10^{17}$ carriers $cm^{-3}$). The samples were cleaved in pieces of 0.5 cm × 0.8 cm, degreased by sonicating in acetone, isopropanol and methanol, rinsed with deionized water and dried in a nitrogen stream. Backcontact to the InSb electrodes was established by smearing InGa eutectic. Electrochemical experiments were performed at room temperature in three different electrolytes of various pH: phosphate buffer at pH = 4.4 (0.3 M $NH_4H_2PO_4$), borate buffer at pH = 8.4 (0.075 M $Na_2B_4O_7$ + 0.3 M $H_3BO_3$) and sodium hydroxide at pH = 13 (0.1 M NaOH). All solutions were prepared from analytical grade chemicals and deionized water. Anodic oxide films were grown under galvanostatic conditions. The electrochemical cell

consisted of a conventional three-electrode configuration with Pt gauze as the counter electrode and an Haber–Luggin capillary with a Ag/AgCl electrode as the reference electrode (all potentials in this paper refer to this electrode). The potentiodynamic investigations as well as galvanostatic anodizations were carried out with an EG&G 173 potentiostat. The electrolytes were open to air prior to and during the measurements and the electrochemical cell was placed in a black box in order to avoid non-controlled photoelectrochemical effects.

Chemical composition and thickness of the anodic films were determined by AES using a Physical Electronics (PHI) 650 instrument with a 5 keV electron beam 30° off normal. Depth profiles were performed using a 1 keV Argon ion beam with sputtering at 51° off normal. The peaks analyzed were In (405 eV), Sb (458 eV), O (510 eV) and the relevant ions, i.e., P (123 eV) and B (185 eV), respectively, for phosphate and borate buffers. Sensitivity factors for In and Sb in the oxides were determined from a 50:50 mixture of $In_2O_3$ and $Sb_2O_3$ and the values were not much different from those provided by the instrument manufacturer's handbook [19] (Different factors apply for the InSb substrate).

X-ray photoelectron spectroscopy was used to identify the species in the anodic film. The XPS system was a Physical Electronics (PHI) 5500 instrument with a monochromatic Al $K_\alpha$ X-ray source and a multi-channel hemispherical detector with an analyzer pass energy of 11.75 eV. The take-off angle was 70° in order to enhance the signal from components closer to the substrate interface.

Roughness measurements were performed using an atomic force microscope (Nanoscope IIIa from Digital Instruments). These measurements were carried out in tapping mode and the root mean square (RMS) roughness was determined using the manufacturer's software. SEM examination was carried out using a Hitachi S-4700 field emission SEM. TEM measurements were performed with a Philips EM 430T operating at 250 keV; cross-sectional samples were made by ion milling.

Electrical characterization was performed on oxide films grown in the three different electrolytes described above. Capacitors were made by depositing aluminium dots, $\approx 5\times10^{-4}$ cm$^2$ on samples through a mask and back contacts were made with InGa eutectic. The current–voltage ($I$–$V$) characteristics were determined using a probe station with a Hewlett–Packard Model 4140B picoammeter-DC voltage source.

## 3. Results and discussion

### 3.1. Electrochemical investigations

Fig. 1(a) shows anodic polarization curves from −1 to 4 V (vs. Ag/AgCl) for highly doped n-InSb substrates in sodium hydroxide, borate buffer and phosphate buffer. As expected the open circuit potential is shifted to negative values (from −0.3 to −0.7 V) with increasing pH. In all cases, the polarization curves in the anodic direction reach a plateau of 0.03–0.1 mA/cm$^2$. In the steady state, which depends on the electrolyte, growth of a surface oxide occurs and a balance between the growth and the dissolution of the oxide film is established. The passive current densities in

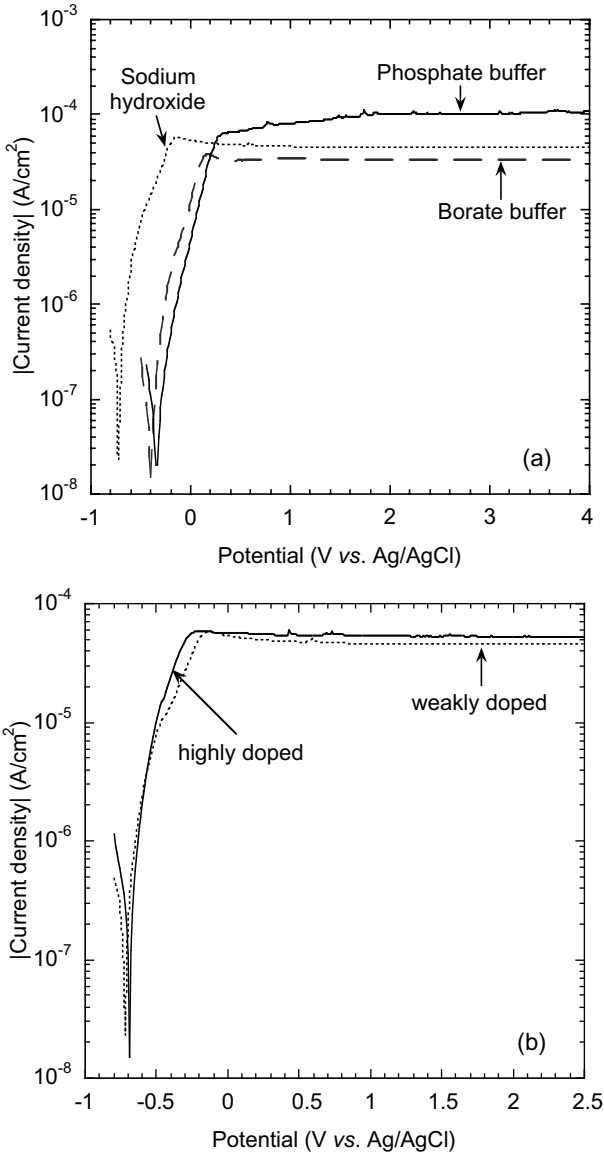


Fig. 1. (a) Anodic polarization curves from −1 to 4 V (vs. Ag/AgCl) for highly doped n-InSb in 0.1 M NaOH (· · ·), borate buffer (– – –) and phosphate buffer (—). (b) Anodic polarization curves from −1 to 2.5 V (vs. Ag/AgCl) for doped (—) and undoped (· · ·) InSb in NaOH (0.1 M). Scan rate was 10 mV/s.

borate buffer, sodium hydroxide are clearly lower than in phosphate buffer, indicating the presence of a better quality oxide.

Fig. 1(b) shows anodic polarization curves recorded on undoped and doped InSb substrates in NaOH (0.1 M). It is clear that there is no significant difference between

the two types of samples. This must be ascribed to the low band gap of InSb (0.17 eV at room temperature) that makes the materials in electrochemical experiments to behave similar to a metal. This was confirmed by illumination experiments where it was found that the current–voltage characteristic did not exhibit any significant variation with white-light illumination. For the sake of clarity polarization curves performed in phosphate and borate buffer are not shown in Fig. 1(b) but no significant variation between the doping levels was again observed. Based on these findings, further experiments were conducted with the doped material.

### 3.2. Auger analysis

Fig. 2 shows the Auger depth profiles for oxides formed in the three solutions. All oxides are In rich and the In and Sb levels are quite uniform in the oxide formed in sodium hydroxide (a) and borate buffer (b). Traces of boron are found in the oxide formed in borate. Phosphorus is detected in the oxide formed in phosphate buffer (c), particularly in the outer part of the oxide where the Sb content increases.

Fig. 3 presents the change in oxide thickness measured from the AES profiles (Fig. 2) as a function of the applied current density. For the same current density, thicker films are obtained in sodium hydroxide than in borate buffer and phosphate buffer. From this comparison it is clear that the pH has a strong effect on the film thickness. AES profiles were also used to determine the rate of oxide growth. From Fig. 4 it is apparent that the oxide thickness evolves linearly with time in the three electrolytes. This is in agreement with the kinetic model for anodic oxidation growth described in the literature [20] where the oxide layer grows at constant voltage. The oxide rate of growth is 0.6, 0.8 and 0.9 nm/s with an applied current density of 1 mA/cm$^2$ in phosphate buffer, borate buffer and sodium hydroxide, respectively.

### 3.3. XPS analysis

For chemical state identification high-resolution peaks of In $3d_{5/2}$, Sb 4d and O 1s (with overlapping Sb $3d_{5/2}$) were used for analysis of samples obtained in all solutions (NaOH, borate, and phosphate). The C 1s peak was set as a reference at a binding energy, BE = 285.0 eV. According to the results of the XPS analysis, all samples showed $In_2O_3$ as the main oxide component, the presence of $Sb_2O_3$, and the total absence of $Sb_2O_5$. A phosphate layer is formed in the outer part of the oxide film in phosphate buffer, which is confirmed in XPS analysis by the P 2p doublet at $BE_{3/2} = 33.5$ eV and $BE_{1/2} = 134.4$ eV. As noted earlier, P is also seen in the outer layer by Auger. A small XPS peak at BE = 191.6 eV suggests that some boron is incorporated in the outer part of the film formed in borate buffer solution, again confirming the Auger observation.

Fig. 5 presents the fitted In $3d_{5/2}$ (a), O 1s (and Sb $3d_{5/2}$) (b) and Sb 4d (c) peaks of the oxide film obtained in 0.1 M NaOH solution. The position of each component was confirmed by data from $In_2O_3$, $Sb_2O_3$ and $In(OH)_3$ Puratronic standards pressed into In foil. In Fig. 5(a) the main component $In_2O_3$ has a BE = 444.8 eV. A very small contribution from $In(OH)_3$ appears at a BE = 445.7 eV. Fig. 5(b) shows a

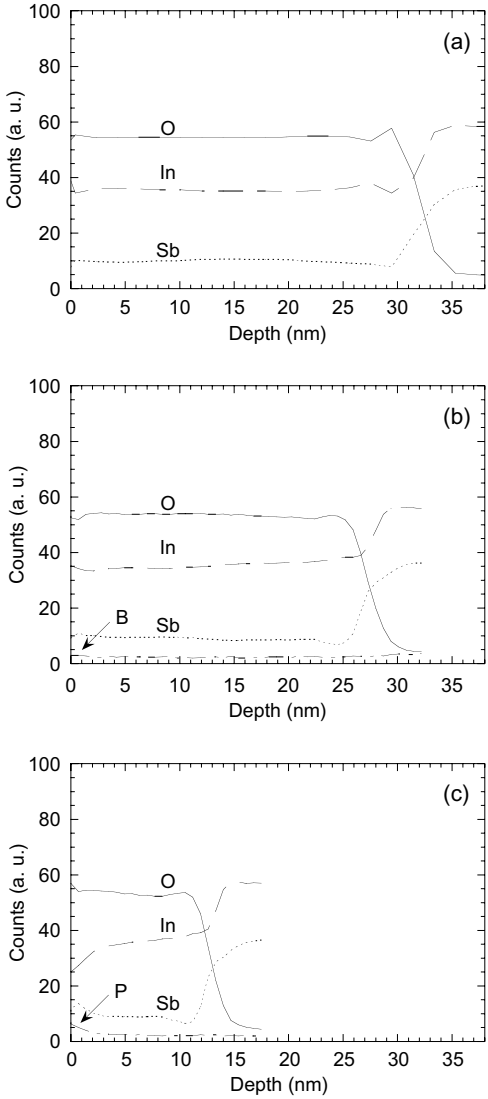


Fig. 2. AES depth profiles performed on oxide films grown on n-InSb in NaOH (a), borate buffer (b) and phosphate buffer (c) at 0.5 mA/cm$^2$ for 60 s. Sputtering was by 1 keV argon.

complex combination of the overlapping O 1s and Sb $3d_{5/2}$ peaks. The main oxides are $In_2O_3$ and $Sb_2O_3$ at a BE = 530.2 eV and a small hydroxide ($In(OH)_3$) contribution at a BE = 531.5 eV. The Sb 4d doublet (Fig. 5(c)) confirms the presence of $Sb_2O_3$ at a $BE_{5/2} = 34.0$ eV and a $BE_{3/2} = 35.2$ eV, respectively.

In summary, the results from the XPS analysis are consistent with previous data [16] and with the results from the Auger profiles described earlier.

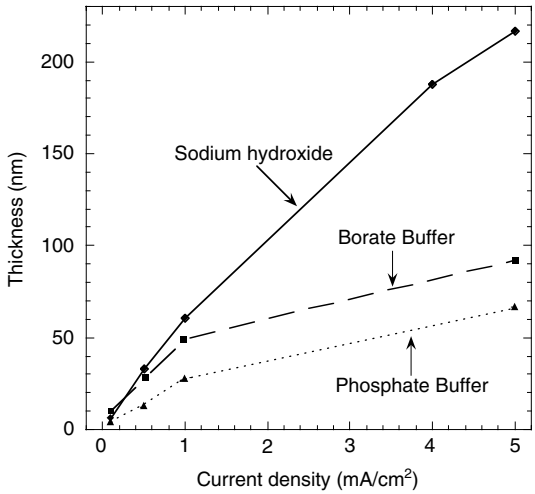


Fig. 3. Thickness of the oxide films vs. the applied current density. Samples were anodized for 60 s in sodium hydroxide (—), borate buffer (– – –) and phosphate buffer (· · ·). Oxide thickness was determined from the sputter time in AES depth profiles when the oxygen signal fell to 50%; sputtering rates were calibrated by TEM cross-sectional measurements of the oxide films (cf. Fig. 8).

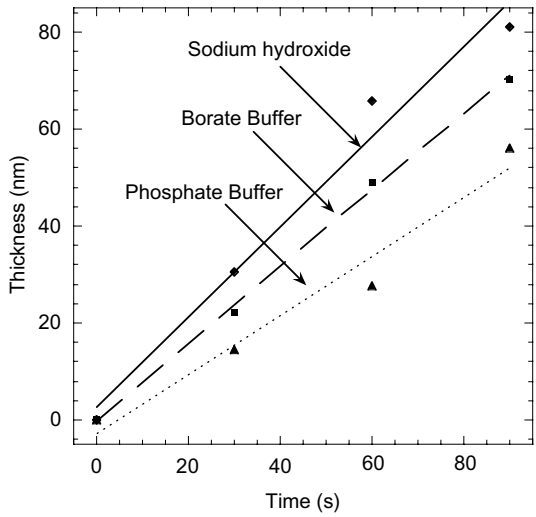


Fig. 4. Thickness of the oxide films vs. time. An anodic current density of 1 mA/cm$^2$ was applied to the samples in sodium hydroxide (—), borate buffer (– – –) and phosphate buffer (· · ·).

### 3.4. Oxide morphology

Root mean square roughness ($R_{RMS}$) measurements were made using AFM in the tapping mode. Fig. 6 shows the surface of InSb oxidized in phosphate buffer (a),

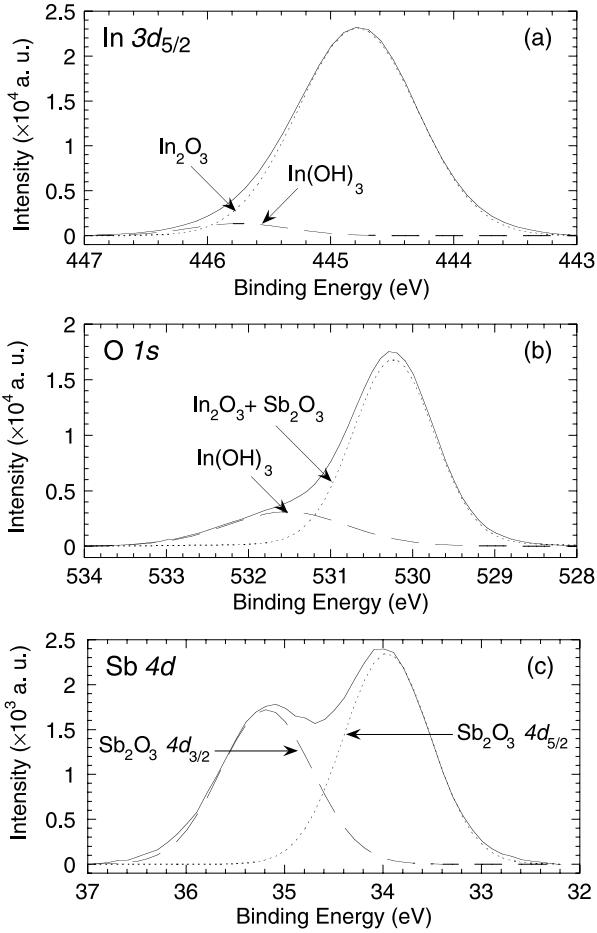


Fig. 5. Deconvoluted In $3d_{5/2}$ (a), O 1s (and Sb $3d_{5/2}$) (b) and Sb 4d (c) XPS peaks of the oxide film obtained in 0.1 M NaOH at 0.5 mA/cm$^2$ for 60 s.

borate buffer (b) at 0.1 mA/cm$^2$ for 60 s and in sodium hydroxide (c) at 5 mA/cm$^2$ for 60 s. Quite a smooth surface is obtained in phosphate buffer and borate buffer ($R_{RMS}$ values of 0.7 and 0.8 nm respectively). In the case of sodium hydroxide rougher oxide films were obtained. From Fig. 6(c) it is apparent that the oxide grains are quite large in NaOH ($\varnothing \approx 300$ nm) and some features of approximately 50 nm are present on the top of the oxide layer (here $R_{RMS} = 11$ nm). An SEM cross-section was also made on such a sample (see Fig. 7), which illustrates the roughness of the oxide, the presence of porosity and the stress in the film. This can explain the higher trend, observed in Fig. 3, for oxide layers grown in NaOH as compared to the other electrolytes.

TEM cross-sections presented in Fig. 8 were used to calibrate the AES profiles shown earlier. From these micrographs, it is apparent that the InSb/oxide interface is

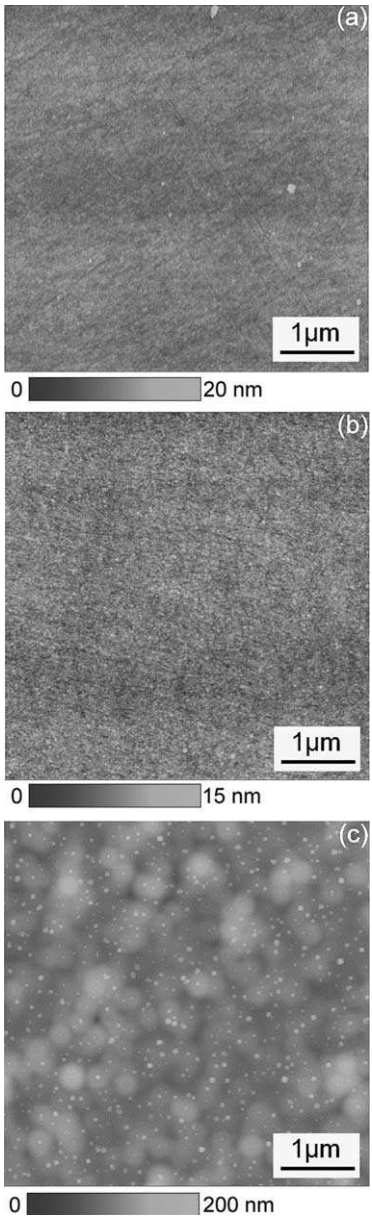


Fig. 6. AFM top views of oxide films on n-InSb by galvanostatic anodization ($i = 0.1$ mA/cm$^2$) in phosphate buffer (a), borate buffer (b) and ($i = 5$ mA/cm$^2$) in sodium hydroxide (c).

well defined and the oxide films are uniform in thickness. It is noteworthy to see the large number of dislocations in the substrate which could negatively affect the electrical measurements of the quality of the oxide films. High-resolution TEM

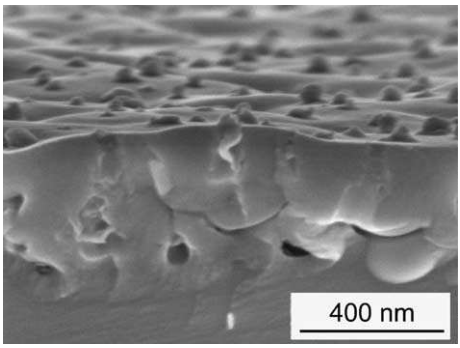


Fig. 7. SEM cross-section of oxide film formed in NaOH (0.1 M) at 5 mA/cm$^2$ for 60 s.

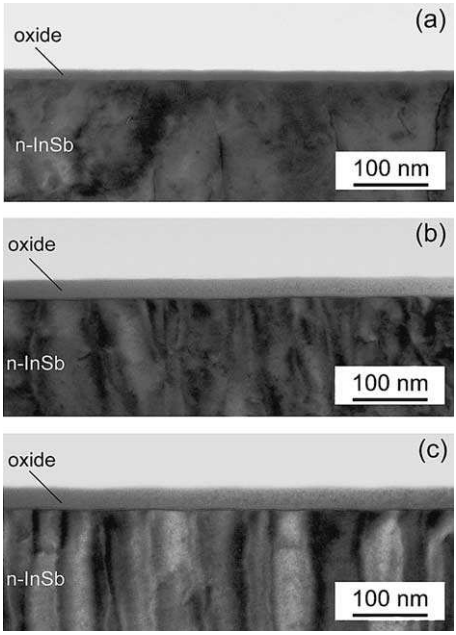


Fig. 8. TEM cross-sections produced by ion milling of oxide films formed at 0.5 mA/cm$^2$ for 60 s in phosphate buffer (a), borate buffer (b) and sodium hydroxide (c).

observation (Fig. 9) of the oxide layer presented in Fig. 8(c) shows clearly that the oxide film is amorphous with some nanocrystallites visible within the film.

### 3.5. Dielectric characterization

Electrical measurements were performed on oxide films grown in the three different electrolytes at 1 mA/cm$^2$ for 60 s and at 0.1 mA/cm$^2$ for 180 s in borate buffer.

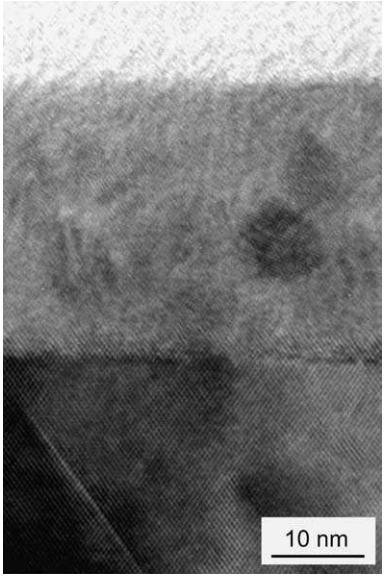


Fig. 9. High-resolution TEM micrograph of the oxide layer presented in Fig. 8(c).

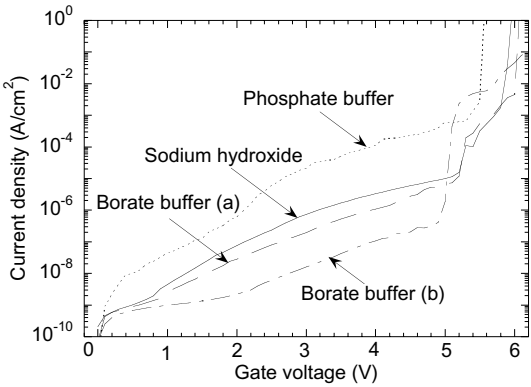


Fig. 10. Variation of the current density vs. the gate bias voltage for injection from the gate for oxide layers formed on n-InSb under various conditions: applied current was 1 mA/cm$^2$ for 60 s in (0.1 M) NaOH (—), phosphate buffer (· · ·), (a) borate buffer (– – –) and (b) 0.1 mA/cm$^2$ for 180 s in borate buffer (– · – · –).

The current density is shown in Fig. 10 as a function of voltage applied to the gate of the metal insulator semiconductor (MIS) capacitor. The breakdown voltages as well as the breakdown fields are given in Table 1. The values obtained demonstrate that the films may be useful as insulators in some device applications. By comparing the values of the breakdown field for oxide films made in borate buffer at various current densities, it appears that the insulating properties are better for higher current

Table 1
Dielectric performances of the oxide films grown under various conditions

| Electrolyte | Current density ($mA/cm^2$) | Duration (s) | Thickness (nm) | Breakdown field (MV/cm) |
|---|---|---|---|---|
| NaOH (0.1 M) | 1 | 60 | 70.7 | 0.7 |
| Phosphate buffer | 1 | 60 | 49.0 | 1.1 |
| Borate buffer | 1 | 60 | 27.6 | 1.8 |
| Borate buffer | 0.1 | 180 | 48.0 | 1.1 |

densities. The ramped *I–V* characteristics were obtained at a ramp rate of 0.1 V/s since leakage currents were low enough, in the 0.2–0.5 V range, to determine the quasistatic capacitance and the resulting dielectric constant. The dielectric constant determined for this oxide formed in borate at 1 $mA/cm^2$ was $14.0 \pm 5$.

## 4. Conclusions

1. Anodic films formed in sodium hydroxide (pH 13), borate buffer (pH 8.4) and phosphate buffer (pH 4.4) comprise mainly $In_2O_3$ and $Sb_2O_3$. The thickness of the oxide increases with pH. Some boron and phosphorus incorporation occurs in borate and phosphate, respectively.
2. The level of doping and sample illumination with white light had little effect on the oxide growth rate.
3. Electrical properties of the uniformly thick oxides indicate that the films may be useful as insulators in some device applications. Films formed in borate buffer at 1 $mA/cm^2$ exhibited breakdown fields of 1.8 MV/cm and a dielectric constant around 14.

## Acknowledgements

The authors thank J. Fraser, J. Phillips and H.-W. Chen for technical assistance. The BMBF is acknowledged for financial support through the Canada/Germany Cooperative R&D Agreement. L. S. would also like to thank the Swiss National Foundation (SNF) for financial support.

## References

[1] C.W. Wilmsen, Physics and Chemistry of III–V Compound Semiconductor Interfaces, Plenum, New York, 1985.
[2] H. Hasegawa, H.L. Hartnagel, J. Electrochem. Soc. 123 (1976) 713.
[3] C.W. Fischer, S.W. Teare, J. Appl. Phys. 67 (1990) 2608.
[4] C.D. Maxey, M.U. Ahmed, C.L. Jones, R.A. Catchpole, P. Capper, N.T. Gordon, M. Houlton, T. Ashley, J. Electron. Mat. 30 (2001) 723.
[5] C.-Y. Wei, H.H. Woodburry, S.C.-H. Wang, IEEE Trans. Electron Dev. 37 (1990) 611.
[6] S.L. Tu, W.H. Lan, T.S. Chion, S.J. Yang, K.F. Hung, Jpn. J. Appl. Phys. 29 (1990) L398.

[7] Y. Shapira, J. Bregman, Z. Calahorra, R. Goshen, Thin Solid Films 89 (1982) 401.
[8] P. Schmuki, G.I. Sproule, J.A. Bardwell, Z.H. Lu, M.J. Graham, J. Appl. Phys. 79 (1996) 7303.
[9] P. Schmuki, R.J. Hussey, G.I. Sproule, Y. Tao, Z.R. Wasilewski, J.P. McCaffrey, M.J. Graham, Corros. Sci. 41 (1999) 1467.
[10] T. Djenizian, G.I. Sproule, S. Moisa, D. Landheer, X. Wu, L. Santinacci, P. Schmuki, M.J. Graham, Electrochim. Acta 47 (2002) 2733.
[11] C.C. Chang, B. Schwartz, S.P. Murarka, J. Electrochem. Soc. 123 (1977) 922.
[12] W.S. Chan, J.T. Wan, J. Vac. Sci. Tech. 14 (1977) 718.
[13] C.W. Wilmsen, Thin Solid Films 46 (1977) 17.
[14] M.J. Mattausch, D.E. Aspnes, Phys. Rev. B 23 (1981) 1896.
[15] Y. Shapira, J. Bregman, Z. Calahorra, Appl. Phys. Lett. 46 (1985) 48.
[16] A. Rastogi, K.V. Reddy, Thin Solid Films 270 (1995) 616.
[17] J.F. Dewald, J. Electrochem. Soc. 104 (1957) 244.
[18] C.W. Wilmsen, J. Vac. Sci. Tech. 13 (1976) 64.
[19] L.E. Davis, N.C. MacDonald, P.W. Palmberg, G.E. Riach, R.E. Weber, Handbook of Auger Electron Spectroscopy, second ed., Physical Electronics Industries, Eden Prairie, MN, 1972.
[20] S.P. Grinberg, Y. Shapira, Z. Calahorra, Phil. Mag. Lett. 55 (1987) 305.